Temperature and velocity boundary layers in turbulent convection

Andrew Belmonte, Andreas Tilgner,* and Albert Libchaber†
Department of Physics, Joseph Henry Laboratories, Princeton University, Princeton, New Jersey 08544
(Received 10 December 1993)

We experimentally study the temperature and velocity fields in high Rayleigh number (Ra) convection by making local measurements as a function of distance from the boundary in a cubic cell. The experiments are performed at two different Prandtl numbers (Pr). In water (Pr=6.6), we measure the thermal and viscous boundary layers for Ra= 1×10^9. We also estimate the advective heat transport in the cell. In room temperature gas (Pr=0.7), we measure the thermal boundary layer for Ra from 5×10^5 to 1×10^{11}. Its thickness scales as $\mathrm{Ra}^{-2/7}$ for Ra > 2×10^7. We measure a second length scale at both Pr using the maximum cutoff frequency of the power spectrum, and demonstrate that it corresponds to the maximum velocity of the large scale circulation. In the gas, this length is consistent with a $\mathrm{Ra}^{-1/2}$ scaling for Ra > 2×10^9. We also present the temperature skewness and the effects of Pr.

PACS number(s): 47.27.Nz, 47.27.Te

I. INTRODUCTION

Two of the main phenomena in turbulent Rayleigh-Bénard convection are a power law dependence of the dimensionless heat flux (Nu) on Rayleigh number (Ra) [1–4], and a persistent large scale circulation, the velocity of which also scales with Ra [3,5,6]. These phenomena have been observed up to the highest Ra achieved ($\sim10^{14}$) through measurements of heat flux, local temperature fluctuations in the cell, and visualization. The heat flux is determined by thermal boundary layers at the top and bottom plates, and the large scale circulation produces viscous boundary layers at the walls. To study these layers directly, local measurement of temperature and velocity must be made at different distances from the surfaces. Previous such studies in turbulent convection did not illuminate these phenomena, as they were made in a limited range of relatively low Ra [7]. We were thus motivated to measure the temperature and velocity boundary layers.

The experimental consensus on the scaling law $\mathrm{Nu}\sim\mathrm{Ra}^{\alpha}$ is that $\alpha\sim0.28-0.30$, about $\frac{2}{7}$. The measured values are clearly different from $\frac{1}{3}$, which is predicted by assuming that the thermal boundary layer is determined by self-instability, and is therefore independent of the cell height L [8]. $\alpha=\frac{2}{7}$ implies that the thermal layers does depend on L. Since the large scale circulation is an eddy of size L, it may pertain to the scaling of Nu. This has been taken into account in a model which derives the $\frac{2}{7}$ scaling, and the velocity scaling, by explicitly including a shear at the wall [9]. The relation between heat flux and shear in turbulent convection has been addressed experimentally by artificially shearing the thermal layer in different ways [4,10].

In essence, the problem is to find the relation between the temperature and velocity boundary layers. These two layers are each somehow produced by the thermal instability in the cell, and each plays a role in the transfer of heat between the plates. As we shall show, their thicknesses scale differently with Ra, which may ultimately put a bound on the range of Ra where the $\frac{2}{7}$ law holds for Nu. Our data suggest a $\frac{1}{2}$ power law for the heat flux, imposed by the velocity layer for Ra greater than 10^{14}.

Previous experiments have used helium gas at 5 K to change Ra over many orders of magnitude in the same cell, but the use of moveable probes and flow visualization is difficult in such cryogenic systems. We therefore choose to perform our experiments at room temperature, focusing on the boundary layer near one of the plates in a cell of cubic geometry. By varying the pressure of several gases, we cover a range of Ra from 5×10^5 to 1×10^{11} (Pr=0.7), and measure the thermal boundary layer thickness with movable thermistors [11]. This measurement gives us the local heat flux. Because velocity measurement is difficult in gas, we use water at Ra=1×10^9 (Pr=6.6) and directly measure the viscous layer [12]. The water experiment teaches us that the maximum velocity of the large scale circulation is at the same position as the maximum cutoff frequency of the temperature power spectrum. We then return to the gas and use this cutoff frequency to measure indirectly the location of the maximum velocity, and its dependence on Ra. The observed scaling of the cutoff frequency with Ra confirms its identification with the large scale circulation velocity.

II. THE HEAT FLUX

A. Experimental setup: gas

Let us describe the experimental apparatus for the high-pressure gas experiment. The setup allows for both

*Present address: Physikalisches Institut, Universität Bayreuth, 95440 Bayreuth, Germany.
†Also at NEC Research Institute, 4 Independence Way, Princeton, NJ 08540.

visualization and movable temperature probes. A diagram is shown in Fig. 1. The principle of its design is to allow the pressure inside and outside the convection cell to be the same by containing it within a larger pressure vessel. Some care must be taken to control flow exterior to the cell, and to provide thermal isolation. The pressure vessel is made of 1-in.-thick cold-rolled steel, and is designed to withstand pressure differences of up to 50 atmospheres [13]. It has a cylindrical interior, 16 in. in length and 15.75 in. in diameter. Two endcaps are bolted to flanges on the vessel, making an *o*-ring seal. For visualization, a 2-in.-thick plexiglass window, 11 in. in diameter, is held within each endcap, and sealed by an *o*-ring. The resulting portals permit a circular view of the interior 8.5 in. in diameter.

The cell itself is a cube 15.2 cm on each side, shown in Fig. 2. The top plate is a copper block held at constant temperature by a water circulation bath [14]. Two brass pipes which supply the water pass through the top of the pressure vessel, and suspend the cell. The bottom plate, also of copper, is heated electrically with a constant power [15]. The side walls are made of 1-cm-thick plexiglass. The heating power ranges from 1 to 15 W, resulting in temperature differences (Δ) from 8 to 25 °C, chosen such that the midway temperature is not far from room temperature. The gas surrounding the cell is regulated to be near room temperature, and cotton batting is used to impede any motion and increase thermal isolation. A small hole in the top plate allows the pressure in the vessel and cell to equilibrate.

To scan Ra we change the density of the gas, varying the pressure between 0.6 and 18 atm for three different gases (helium, nitrogen, and sulfur hexafluoride) and staying far from the critical point of each gas. The resulting span of Rayleigh number is almost six decades, from 4×10^5 to 1×10^{11}, while the Prandtl number remains within 5% of 0.7. Experimental values of Ra are calculated using the pressure and temperature dependence of the material properties of each gas [16,17], evaluated at the midway temperature between the plates. Because these properties are not strongly dependent on temperature, the precision in Ra in about 10%. Our experiments are thus within the Boussinesq approximation [18], which assumes that all material properties of the fluid except for the density are temperature independent. We therefore measure only in the upper half of the cell, while verifying that in the bulk that $\langle T\rangle \sim T_{\text{top}}+\Delta/2$.

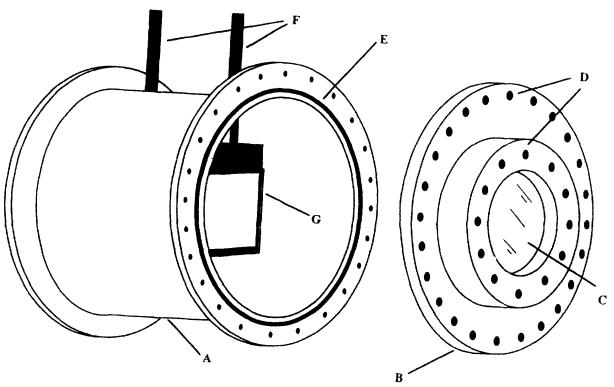

FIG. 1. A diagram of the experimental apparatus for compressed gas: *A*, steel pressure vessel; *B*, endcap; *C*, plexiglass window; *D*, bolts; *E*, *o* ring; *F*, water supply pipes; and *G*, convection cell.

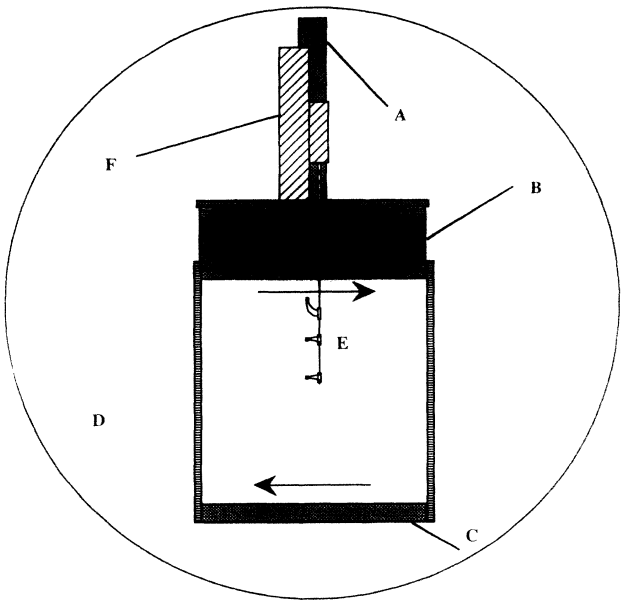

FIG. 2. A diagram of the gas convection cell: *A*, water supply pipes; *B*, top plate; *C*, bottom plate; *D*, exterior filled with cotton; *E*, thermistors on tube (not to scale); and *F*, translation stage. The arrows are drawn to indicate the direction of the large scale circulation near the plates.

The temperature in the cell is measured with uncoated metal oxide thermistors [19] about 200 μm in diameter, with 50-μm-thick leads, and a room-temperature resistance of approximately 20 kΩ. These probes are attached by 250-μm manganin support wires to a 0.9-mm-diameter thin stainless-steel tube, within which the signal wires are passed. The typical Reynolds number of the tube in the flow is about 10, thus a small perturbation. We also arrange the temperature probes so that they are upstream of the tube and wires. The probes are moved by attaching the rube to an electronically controlled microtranslational stage [20] through a small hole in the center of the top plate. This stage has a total travel of 25.4 mm, with a positional accuracy of 4.0 μm. Typically three thermistors are spaced vertically by about 25 mm (as shown in Fig. 2), thus covering the cell from the top plate ($z\equiv0$ mm) to the center ($z=76$ mm).

The thermistor resistance is measured with an ac-driven (1–3 kHz, 0.1 V_{rms}) Wheatstone bridge and a lock-in amplifier [21]. The off-balance voltage of the bridge, ranging from 50 μV to 2 mV peak to peak, is demodulated by the lock-in amplifier, digitized by a spectrum analyzer [22], and stored on disk as a time series. Sampling times range from 1 msec at the highest Ra to 100 msec for the lowest value. The duration of an individual time series at each height varied from 15 min to several hours, depending on Ra.

B. The thermal boundary layer

We study the top boundary layer by varying the distance of the probe from the plate. Measuring the fluctuating temperature at each point, we obtain profiles of the mean ($\langle T \rangle$), root mean squared (RMS) (θ), and skewness (S). Examples of such profiles are shown in Fig. 3. It is evident from the mean profile that about half of the total temperature difference Δ is confined to a region near the plate, the thermal boundary layer. The z dependence of the mean is linear close to the plate, and extrapolates to the plate temperature at $z=0$. We define the boundary layer thickness λ_{th} in the following way: λ_{th} is the distance at which the extrapolation of the linear portion of the mean profile equals the central mean temperature. The mean is linear for about 60% of the thickness of the thermal layer, and the error on λ_{th} due to the extrapolation is about 0.2 mm. A plot of λ_{th} vs Ra is shown in Fig. 4. For $\mathrm{Ra} > 2\times10^7$, we find

$$\lambda_{th} \sim \mathrm{Ra}^{-0.29\pm0.01} .$$

The most striking feature of the RMS profile is its well-defined maximum, with a smooth tail extending to the center of the cell (as in Fig. 3). We discuss this tail in Appendix A. For $\mathrm{Ra} > 2\times10^7$, the maximum is located at λ_{th}; for $\mathrm{Ra} < 2\times10^7$, it is slightly closer to the plate. This maximum at λ_{th} shows that the thermal layer is not a static conducting layer, but a strongly fluctuating structure, as observed in visualizations.

The skewness is defined as $S \equiv \langle (T-\langle T \rangle)^3 \rangle / \langle (T-\langle T \rangle)^2 \rangle^{3/2}$; it is dimensionless. It reaches a broad extremum in the region outside the thermal boundary layer (Fig. 3). The details of the skewness profile are discussed in Appendix A.

The Nusselt number (Nu) is defined as the ratio of the actual heat flux through the cell (J) to the conductive heat flux for the same temperature difference Δ. It is

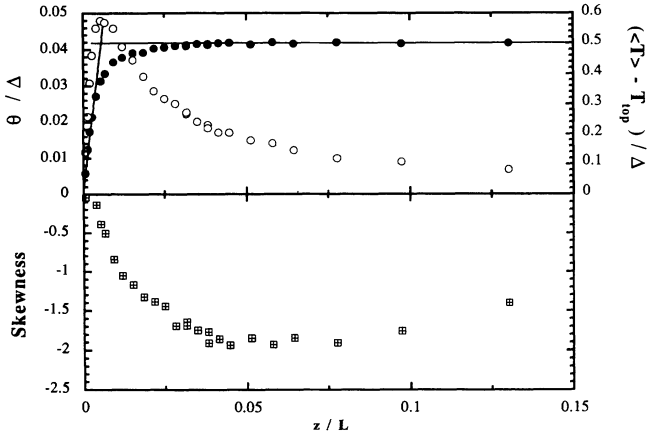

FIG. 3. The temperature mean (black dots), RMS (white dots), and skewness (squares) profiles vs z/L, for SF_6 at $\mathrm{Ra}=3.5\times10^9$ and $\Delta \sim 19\,^{\circ}\mathrm{C}$; $L=15.2$ cm. The mean is normalized as $(\langle T \rangle - T_{top})/\Delta$, so that the top plate and midway temperatures are zero and 0.5, respectively. The lines drawn indicate the linear dependence near the plate and saturation value of $\langle T \rangle$.

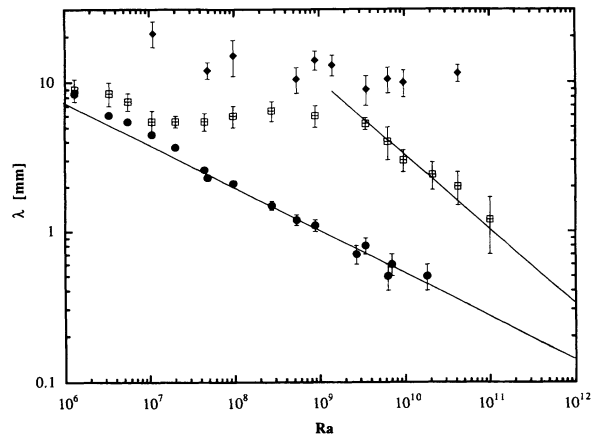

FIG. 4. The thermal boundary layer thickness λ_{th} (circles), the position of the maximum cutoff frequency λ_m (squares), and the position of maximum skewness λ_{sk} (diamonds) vs Ra. The line drawn for λ_{th} corresponds to $\mathrm{Ra}^{-0.29}$; the line for λ_m corresponds to $\mathrm{Ra}^{-1/2}$.

written $\mathrm{Nu} = JL/\chi\Delta$, where χ is the thermal conductivity, and L is the height. Because of the lack of thermal isolation in our apparatus, we cannot measure J. However, the heat flux is also given locally by the temperature gradient at the wall: $J_{loc} = \chi(\partial T/\partial z)|_{wall}$. The definition of λ_{th} leads to $(\partial T/\partial z)|_{wall} = \Delta/(2\lambda_{th})$. We thus write a pointwise Nusselt number as $\mathrm{Nu}_{pt} = L/2\lambda_{th}$; averaging this over the whole plate will yield the total Nusselt number Nu_{tot}. For $\mathrm{Ra} > 2\times10^7$, we find, at the center of the plate,

$$\mathrm{Nu}_{pt} = 0.18\,\mathrm{Ra}^{0.29\pm0.01} .$$

Convection experiments in low temperature helium gas measured the total heat flux in a cell of aspect ratio 1, and found

$$\mathrm{Nu}_{tot} = 0.22\mathrm{Ra}^{0.285\pm0.004}$$

for $\mathrm{Ra} > 4\times10^7$ [3,6]. The two Nusselt numbers are plotted in Fig. 5. From this we conclude that the pointwise flux at the center characterizes the total flux for $\mathrm{Ra} > 10^7$,

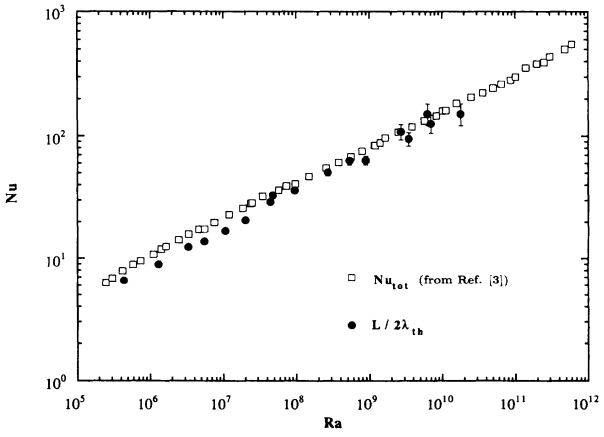

FIG. 5. $\mathrm{Nu}_{pt} = L/2\lambda_{th}$ from our measurements, and Nu_{tot} from [3].

which means that $L/2\lambda_{th}$ is a good approximation of the total Nusselt number.

III. THE LARGE SCALE CIRCULATION

The origin of the large scale circulation in turbulent convection is unexplained. Its presence most certainly affects the state of turbulence, and may be the reason for the $\frac{2}{7}$ scaling of the thermal boundary layer. We might even argue that large scale flows introduce a nonuniversal aspect to turbulence, which could be the most fundamental new development in this field. We therefore wanted to measure the Ra dependence of the velocity near the plate. However, a fluctuating velocity in a nonisothermal fluid is notoriously difficult to measure. The measurements of mean velocity which have been made in turbulent convection use two temperature probes placed along the sidewalls of the cell, and measure the mean delay time of the fluctuations [3,6]. This technique is impractical near the fluctuating boundary layer due to the motion of thermal plumes perpendicular to the mean flow. By studying convection in water, at a larger Prandtl number than gas, we give up a large range of Ra in exchange for the capacity to measure velocity by visual techniques. The effects of the Prandtl number are discussed in Appendix B. We describe first the measurement of velocity in water, then an indirect method which can be used in gas.

A. Experimental setup: water

The water cell is a cube 18.3 cm high, with glass sidewalls allowing visual access; it is described in a previous paper [12]. In this experiment, $\mathrm{Ra}=1.1\times10^9$ and $\mathrm{Pr}=6.6$. We measure the velocity as a function of distance z from the center of the plate using the pH dye technique [23]. A pH indicator, thymol blue sodium salt, is dissolved in water at a concentration of 0.02% by weight, with NaOH added to increase the available electrolytes. The indicator is dark blue for pH above 9.6 (basic), and yellow orange at lower pH. The solution is titrated just below pH 8 with HCl. By passing a current through electrodes in the cell, the pH is increased in the neighborhood of the cathode (positive), causing the indicator to change color in that region. The formation of gas bubbles at the cathode can be avoided,if the current is low enough.

To measure local velocity, we use the bare tip of a coated 150-μm-thick manganin wire as the cathode, and one of the plates as the anode. The wire is moved below the top plate by a stainless-steel tube 190 μm in diameter, which has an estimated Reynolds number in the flow of 2. Square pulses typically 5 V in amplitude and $\frac{7}{60}$ sec in duration are sent through the wire, marking the fluid in the vicinity of the wire tip with blue dye. We evaluate the velocity at the wire tip by measuring the distance that the dyed fluid travels in one second; the motion is observed to be uniform for at least this interval [12]. The resulting measurement is of the component of velocity normal to the line of sight.

The dyed fluid is imaged by a CCD camera against a diffuser illuminated by a sodium vapor lamp to improve contrast. The video output of the camera is then digitized by computer. The real-time display on the computer is stopped 1 sec after the pulse is applied to the wire, and a human operator records the position of the dark blob on the screen using a mouse. The velocity is measured every 3 sec with this technique, and a typical time series lasts from 15 to 30 min, limited by operator fatigue.

B. Velocity near the wall

Using this technique we measure the fluctuating velocity in the vertical and horizontal directions as a function of height [12]. The histograms of the horizontal velocity are Gaussian through most of the cell; an example is shown in Fig. 6. The mean horizontal velocity U is plotted vs height in Fig. 7. Its dependence on z is linear close to the plate, extrapolating to zero at $z=0$. We define the thickness of the viscous boundary layer λ_v as the point at which the extrapolation of the linear part of the profile equals the maximum velocity of U. We find that $\lambda_v=3.8\pm0.4$ mm. Further away from the plate, the velocity U reaches a maximum at 9 ± 2 mm. This means that the large scale circulation produces a jet along the plate, with its maximum velocity at about 5% of the cell height L.

The vertical velocity histograms are also Gaussian and centered close to zero, except near the boundary, where there is a skewness towards movement away from the plate, as shown in Fig. 6. The mean vertical velocity V is less than 10% of of the horizontal mean U at all heights. For $z/L\sim0.4-0.6$, we find that U and V are small compared to the velocity fluctuations, and the histograms of the vertical and horizontal velocities have the same shape: the velocity field is homogeneous and isotropic in this region.

We also measure the local temperature fluctuations and their position dependence, as described in a previous paper [12]. From this we find that $\lambda_{th}=1.9\pm0.3$ mm, and $\mathrm{Nu}_{pt}=48\pm6$. By looking at the power spectrum of the temperature fluctuations in water, we discovered a fingerprint of the velocity field.

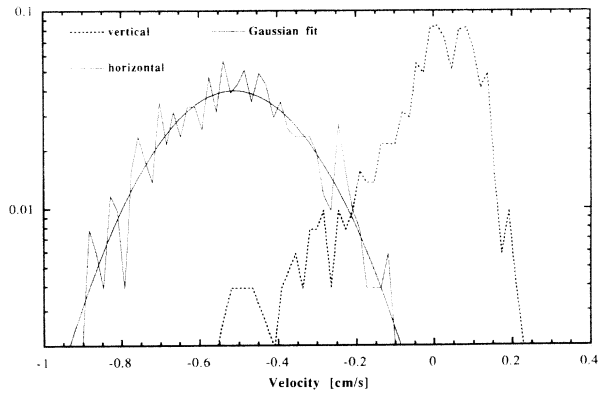

FIG. 6. Histograms of the vertical and horizontal velocities for water at $\mathrm{Ra}=1.1\times10^9$ and $\Delta=10\,^\circ$C, at $z/L=0.033$; the thick line is a fitted Gaussian distribution.

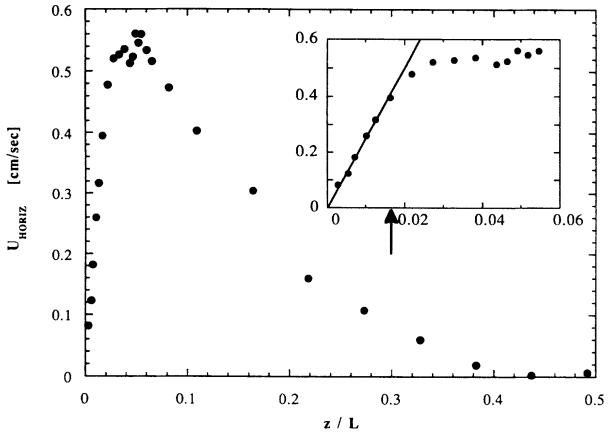

FIG. 7. Profile of the mean horizontal velocity for water at $Ra=1.1\times10^9$; the arrow in the inset indicates the edge of the viscous boundary layer.

C. The cutoff frequency in water and gas

We measure the position of the maximum velocity with a single temperature probe by using the Fourier power spectrum of the fluctuating temperature. The power spectrum has been the subject of much previous research in turbulent convection [24]. In our experiments, we noted as an inconvenience that the spectral extent of the temperature fluctuations changed with the height of the probe. We define *the cutoff frequency* (f_c) as the frequency where the power spectrum of the signal intersects the noise level of the experiment, as indicated for water in Fig. 8. This is a somewhat arbitrary but reproducible measure of the high frequency extent of the spectrum; the signal-to-noise ratio is approximately constant during measurements. In water, we find that f_c reaches a maximum at a position λ_m outside the thermal boundary layer. By plotting the profile of f_c with height, we find that it parallels the mean velocity profile, and that the location of the maximum cutoff frequency, $\lambda_m \sim 10$ mm, corresponds to the location of the maximum velocity of the large scale circulation, as shown in Fig. 9.

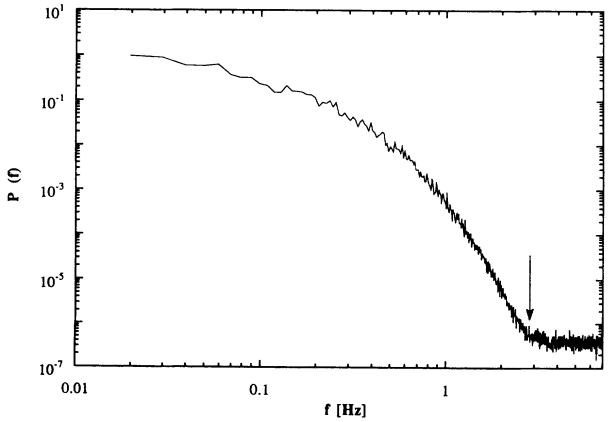

FIG. 8. The temperature power spectrum $P(f)$ at $z/L=0.08$, for water at $Ra=1.1\times10^9$; the arrow indicates the cutoff frequency.

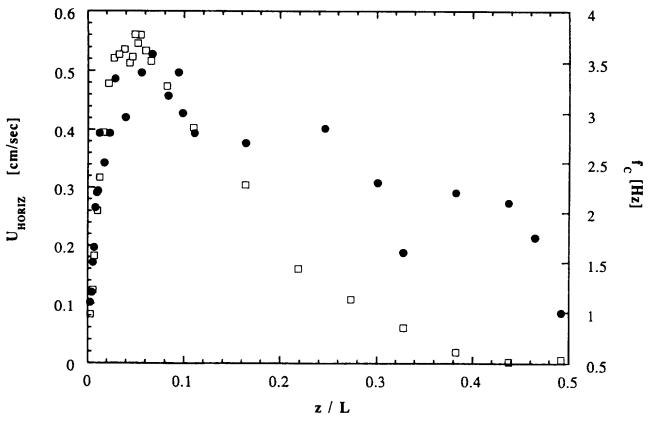

FIG. 9. Profiles of the cutoff frequency (black dots) and the mean horizontal velocity (white squares) for water at $Ra=1.1\times10^9$.

Having made this association in water, we return to gas. We measure f_c as a function of height at each Ra and find that, for $Ra>1\times10^6$, each profile reaches a well-defined maximum at some position λ_m. A typical profile is shown in Fig. 10, for $Ra=1.0\times10^{11}$ [25]. We plot λ_m against Ra in Fig. 4, along with the thermal boundary layer thickness. One immediately sees that the two lengths become separated for $Ra>2\times10^7$, by as much as a factor of 7 for $Ra\sim10^9$. In addition, the Ra dependence of λ_m changes at $Ra=2\times10^9$. There is clearly something to be learned from the interplay of these two lengths.

The actual value of the maximum cutoff frequency, f_{cMAX}, increases with Ra, as shown in Fig. 11. The significance of this increase is discussed below. With both the value of the maximum and its position, we can normalize the profiles at each Ra, and plot f_c/f_{cMAX} vs z/λ_m, as shown in Fig. 12. All of the profiles fall onto a similar curve, leading us to the conclusion that the shape of the f_c profile is also a physical measurement of the flow. We do not have an interpretation for this shape, although it qualitatively resembles the mean velocity profile.

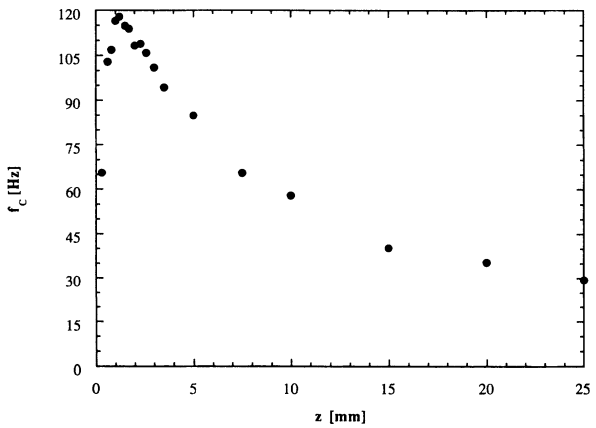

FIG. 10. Profile of the cutoff frequency for gas at $Ra=1.0\times10^{11}$.

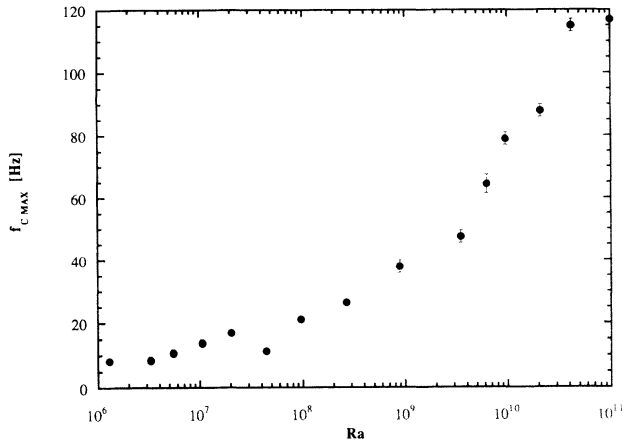

FIG. 11. A plot of the magnitude of f_{cMAX} vs Ra for gas.

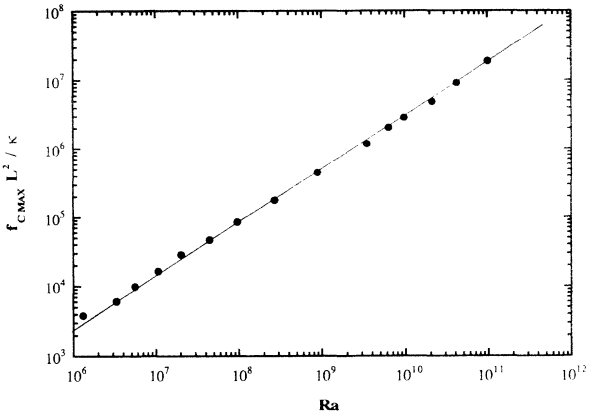

FIG. 13. A plot of $(f_{cMAX}L^2/\kappa)$ vs Ra; the line corresponds to $\mathrm{Ra}^{11/14}$.

We can justify the observed relation between the velocity maximum and the cutoff frequency maximum in the following way. We know that the large scale circulation supplies the dominant mean velocity (U) in the region close to the plates; U must be zero at the plate and at the center of the cell, and therefore must have a maximum in between. Near the top plate, where our measurements are made, boundary layer detachments are advected past the detector, producing sharp fluctuations toward lower temperatures. The temporal width of these peaks in the time series is determined by two things: the spatial width of the gradient in the detachments (Λ), and their advection speed (U). The higher frequencies of the power spectrum originate in the narrower peaks. The cutoff frequency is then written as $f_c \sim U/\Lambda$. Based on observation we know that the typical length scale for detachments near the boundary layer is independent of height, and is approximately λ_{th} [26]. Therefore $f_c \sim U/\lambda_{th}$, and U and f_c are maximum at the same height.

We observe a well-defined scaling of the magnitude of f_{cMAX} which confirms this reasoning. We find that

$$\frac{f_{cMAX}L^2}{\kappa} \sim \mathrm{Ra}^{0.79\pm0.03}$$

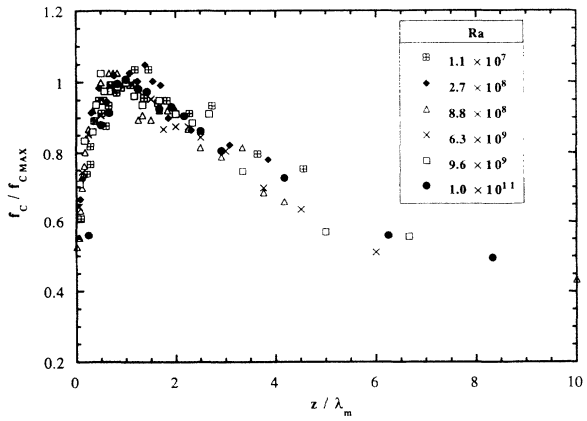

FIG. 12. The cutoff frequency profiles for gas at several values of Ra: f_c/f_{cMAX} vs z/λ_m.

from $\mathrm{Ra}=4\times10^6$ to the highest Rayleigh number we attained (1×10^{11}), as shown in Fig. 13. We derive this exponent using the experimental scalings of the thermal boundary layer and the mean advection velocity [3]:

$$f_{cMAX} \sim \frac{U}{\lambda_{th}} \sim \frac{\mathrm{Ra}^{1/2}}{\mathrm{Ra}^{-2/7}} \sim \mathrm{Ra}^{11/14} .$$

This exponent (0.786) is in agreement with the observed one [27].

IV. DISCUSSION

Let us discuss the temperature and velocity measurements in gas. Having measured the dependence of λ_m and λ_{th} on the Rayleigh number, we divide the measurements into three regimes (see Fig. 4). In the lowest regime ($\mathrm{Ra}<2\times10^7$), we find $\lambda_m \sim \lambda_{th}$, suggesting that both length scales are determined by the same physical process. The other regimes, were $\lambda_{th} \sim \mathrm{Ra}^{-2/7}$, are characterized by a gap that opens between the two length scales, due to the dependence of λ_m on Ra. In one regime ($2\times10^7 < \mathrm{Ra} < 2\times10^9$), $\lambda_m \sim$const, at about 4% of the cell height. Since the magnitude of the circulation velocity increases as $U \sim \mathrm{Ra}^{1/2}$[3], the Reynolds number of this layer,

$$\mathrm{Re}_\lambda = U\lambda_m/\nu ,$$

increases with Ra. We estimate Re_λ to go from 50 at $\mathrm{Ra}=2\times10^7$ to about 600 at $\mathrm{Ra}=2\times10^9$ [11].

Finally, in the highest Ra regime ($\mathrm{Ra}>2\times10^9$), λ_m decreases as $\mathrm{Ra}^{-0.44\pm0.09}$. If we approximate this as $\lambda_m \sim \mathrm{Ra}^{-1/2}$, it implies that Re_λ remains at 600 as Ra increases. Reynolds numbers of this order are typical of turbulent boundary layers. However, we are unaware of any observation of a turbulent boundary layer which adjusts its thickness to maintain a constant Reynolds number. Let us remark that in our case the boundary condition for the forcing velocity far from the wall is not well defined; it is certainly not the boundary condition of a turbulent wind tunnel. The origin and stability of the

large scale flow is thus at the core of the problem of thermal turbulence.

Because our measurement of the maximum velocity is indirect, we should be somewhat cautious about our interpretation. A different interpretation [28] is that the observed decrease of λ_m for $\mathrm{Ra} > 2\times10^9$ is due to a turbulent mixing length z_t, defined by $\mathrm{Re}_{\mathrm{crit}} = Uz_t/\nu$; this mixing shreds the boundary layer detachments. The position of maximum velocity does not change at $\mathrm{Ra}\sim10^9$, and has only a weak dependence on Ra, but the length scale Λ of the detachments is ill defined for all $z > z_t$. Thus the maximum velocity would not be measured via the cutoff frequency, which relies on $f_c \sim U/\Lambda$. The location of $f_{c\mathrm{MAX}}$ then occurs at the mixing distance $z_t = (\nu/U)\mathrm{Re}_{\mathrm{crit}} \sim \mathrm{Ra}^{-1/2}$; in our case $\mathrm{Re}_{\mathrm{crit}} = 600$. One of our difficulties with this explanation is that it does not account for the observation that $f_{c\mathrm{MAX}}$ continues to scale as $\mathrm{Ra}^{11/14}$.

Another possible interpretation also involves mixing due to a turbulent Reynolds number, by estimating the velocity fluctuations [29]. The common element in these interpretations is that for $\mathrm{Ra} > 2\times10^9$, λ_m is characterized by a constant Re_λ, independent of Ra. This indicates that mechanical turbulence is beginning to play a role in turbulent convection.

In conclusion, for $\mathrm{Ra} > 2\times10^9$, λ_m decreases faster than λ_{th}, which implies that the two will cross for Ra above 10^{14}. We suspect that the crossing will change the scaling of the thermal layer, for the following reason: the fact that the velocity maximum is characterized by a turbulent Reynolds number means that there is strong mixing at this position. The thermal layer would then be forced to follow the scaling of λ_m, giving rise to another regime beyond the 2/7, or hard turbulence regime. Postulating that in this regime $\lambda_{\mathrm{th}} \sim \lambda_m$ implies

$$\mathrm{Nu}_{\mathrm{pt}} = \frac{L}{2\lambda_m} = \frac{1}{3870}\mathrm{Ra}^{1/2}\mathrm{Pr}^{-1} .$$

This is close to the scaling predicted by Kraichnan for an eddy-shear-dominated boundary layer at high Ra [30], but in our case the heat flux would be controlled by the large scale circulation. Another regime could then arise when this circulation breaks down. Of course, this is all pure speculation. The experimental facts are that in helium gas, the 2/7 scaling is observed up to $\mathrm{Ra}\sim10^{14}$ [3].

V. CONCLUSIONS

We study the temperature and velocity fields as a function of distance from the top plate for turbulent Rayleigh-Bénard convection in two Boussinesq fluids. We work at two different Prandtl numbers. In water, where a direct measurement of velocity is possible, we measure the thermal and viscous boundary layers at $\mathrm{Ra} = 1\times10^9$. We also define an indirect measurement of the mean velocity via the cutoff frequency. In gas we measure the thermal boundary layer thickness directly, and the position of maximum mean velocity using the maximum cutoff frequency, for Raleigh numbers spanning about five decades up to 10^{11}. For $\mathrm{Ra} > 10^7$, the position of maximum velocity is well outside of the thermal boundary layer. Above $\mathrm{Ra}\sim10^9$, its position decreases such that its Reynolds number (about 10^3) is independent of Ra. Its projected crossing with the thermal layer, at a Rayleigh number above 10^{14}, will change the dynamics of the heat flux through the cell. In order to obtain concrete answers to the questions raised by this paper, we are developing an experiment in room temperature gas to visualize the flow near the boundaries of the cell.

ACKNOWLEDGMENTS

We would like to thank E. Ching, B. Shraiman, E. Siggia, and V. Yakhot for illuminating discussions, and L. Faucheux and D. Fygenson for extensive comments on the manuscript. We would especially like to recognize E. Moses for his early work on this project, including the construction and testing of the pressure vessel. This work was supported by the National Science Foundation under Grant No. DMR 8722714. A.T. acknowledges the support of a NATO grant from the "Deutscher Akademischer Austauschdienst."

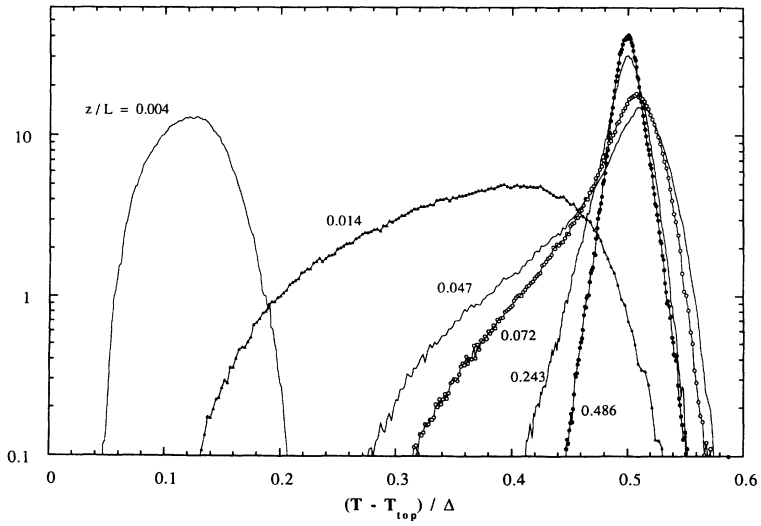

FIG. 14. Temperature histograms for gas at $\mathrm{Ra} = 4.8\times10^7$, for z/L (z/λ_{th}) = 0.004 (0.3); 0.014 (1.0); 0.047 (3.2); 0.072 (5); 0.243 (16.8); and 0.486 (33.5). The y axis is in arbitrary units.

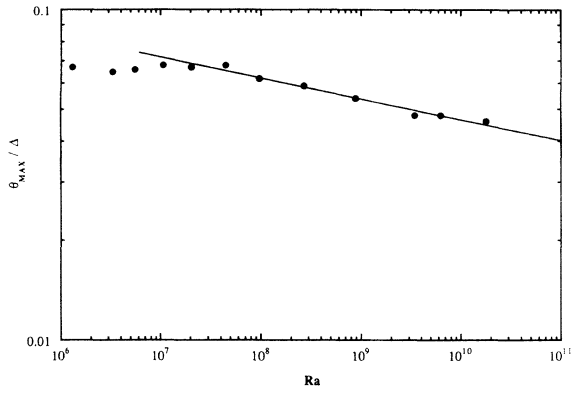

FIG. 15. A plot of θ_{MAX}/Δ vs Ra; the line corresponds to $Ra^{-0.06}$.

APPENDIX A: TEMPERATURE FLUCTUATIONS OUTSIDE THE THERMAL LAYER

Outside the thermal boundary layer, the histograms of temperature fluctuations undergo many changes in shape. In Fig. 14 we show histograms at several positions in the cell, for $Ra=5\times10^7$. The shapes range from a nearly Gaussian shape within the thermal layer to an exponential shape at the center, with the broadest distribution at the edge of the thermal layer. We focus here on the development of the histograms using the RMS and skewness.

Let us recall that the RMS temperature fluctuations peak at the edge of the thermal boundary layer (λ_{th}), and then decrease further into the bulk of the cell. The value of the maximum RMS (θ_{MAX}/Δ) is about 6% in both gas and water, and depends very weakly on Ra in gas (decreasing approximately as $Ra^{-0.06}$ for $Ra>2\times10^7$), as shown in Fig. 15. This means that with increasing Ra, the size of θ_{MAX} does not decrease as rapidly as λ_{th}, so that large fluctuations exist at decreasingly smaller distances. This may ultimately destroy the thermal boundary layer altogether.

The decrease of the RMS outside the thermal layer suggests a universal curve for the fluctuations, seen by

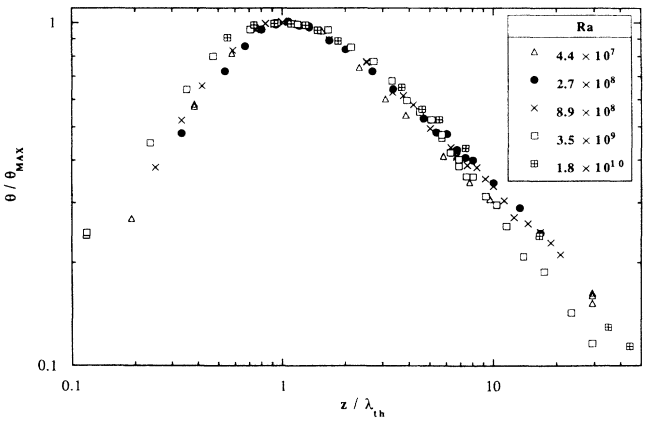

FIG. 16. The RMS profiles for gas at several values of Ra: θ/θ_{MAX} vs z/λ_{th}.

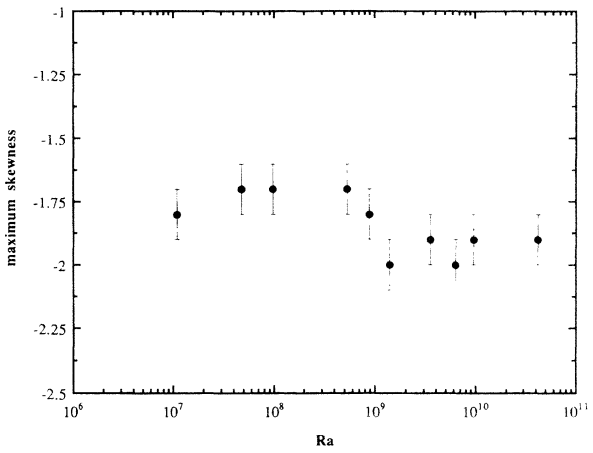

FIG. 17. The maximum skewness of the temperature fluctuations vs Ra.

plotting θ/θ_{MAX} vs z/λ_{th}, as shown in Fig. 16. Our measurements can be fit by a power law $\theta\sim z^{\beta}$ in both gas and water; they are also consistent with $\theta\sim\ln(z)$ in approximately the same region [31,32]. In gas, we find $\beta=-0.72\pm0.09$, a much more rapid decrease than that predicted by Priestley ($\beta=-\frac{1}{3}$) for free convection above a large heated surface [33]. A $\frac{1}{3}$ exponent was also predicted by Kraichnan, but for large Pr; a steeper decrease was anticipated for Pr=0.7 [30]. In water we find $\beta=-0.80\pm0.06$, about the same exponent as in gas. These observations suggest that a universal mechanism exists for the turbulent temperature fluctuations in convection cells of aspect ratio one.

Because of the incomplete thermal isolation in our experiment, small perturbations are introduced which increase as one moves away from the top plate, so that the RMS temperature at the center of the cell is imprecise.

Outside of the top thermal layer (cold), the temperature histograms are asymmetrically skewed toward lower temperatures (see Fig. 14). This indicates that the detachments from the boundary layer are not homogenized; further into the cell the histograms are symmetrical. We measure the asymmetry of the histograms around the mean by calculating the skewness S, defined in the text. We find that there is a position λ_{sk} at which the magnitude of the skewness is maximum. This position is greater than both λ_m and λ_{th} for all of our measurements, and changes very little with Ra ($\lambda_{sk}\sim Ra^{-0.07}$ for $Ra>10^7$). We plot λ_{sk} against Ra in Fig. 4. The value of the skewness at λ_{sk} is plotted in Fig. 17; it is always about -2 (negative skewness corresponds to lower temperature). The fact that the maximum skewness does not change much either in position or magnitude as Ra increases, while the size of fluctuations in the bulk is decreasing, suggests that the basic mechanism producing the fluctuations does not change with Ra. To further connect this observation to the development of the detachments from the thermal boundary layer requires a model for their growth and propagation away from the plate.

An additional signature of the large scale circulation is evident in Fig. 14: there are more warm temperature

fluctuations near the cold plate than at the center. Thus the histogram at $z/L \sim 5\%$ extends further toward the warm than the histograms at 25% or 50%. We conclude that these fluctuations are carried by the circulation along the walls of the cell.

APPENDIX B: PRANDTL NUMBER EFFECTS

The difficulty in measuring Prandtl number (Pr) dependence in turbulent convection is due to the fact that it depends only on the properties of the fluid (but not on density), and thus cannot be varied substantially except by changing fluids. By definition $\mathrm{Pr} \equiv \nu/\kappa$, where ν is the kinematic viscosity and κ is the thermal diffusivity of the fluid. By comparing our two convection experiments at the same Ra, for Pr=0.7 (gas) and 6.6 (water), we get some idea of the effects of Pr. Table I summarizes the measurements we have made in the two experiments at $\mathrm{Ra} = 1 \times 10^9$.

In general, the effect of decreasing Pr at the same Ra is to increase the Nusselt number by increasing the Reynolds numbers of the flow. We find that Nu increases from Pr=6.6 to Pr=0.7, consistent with the scaling $\mathrm{Nu} \sim \mathrm{Pr}^{-1/7}$, a prediction which appears in tandem with $\mathrm{Nu} \sim \mathrm{Ra}^{2/7}$ in all models for hard turbulent convection to date [2,9,32]. However this scaling is not supported by earlier studies which include mercury ($\mathrm{Pr} \sim 0.02$) [34]. It is not known if either $\mathrm{Nu} \sim \mathrm{Ra}^{2/7}$ or a large scale flow occur in mercury.

Outside of the thermal boundary layer, we observe a thermal inversion in the bulk of the cell at Pr=6.6 [12], in agreement with other experiments on water [31,35]. However, we do not observe such an inversion for $\mathrm{Pr} \sim 0.7$ at any Ra.

There are also measurements which are the same for the two Pr we have studied. The maximum RMS temperature ($\theta_{\mathrm{MAX}}/\Delta$) is about 6% of the total temperature difference Δ in both experiments (as well as for all $\mathrm{Ra} > 2 \times 10^7$ at Pr=0.7). The dependence of the RMS on z outside the thermal layer, whether fit as a power law z^{β} or as $\ln(z)$, is approximately the same at both Pr; for the case of the power law we have found $\beta \sim -\frac{3}{4}$. In addition, the position of the velocity maximum λ_m is about 5% of L, a much smaller percentage of the height than had been supposed [9,36]. The dependence of Reynolds number and of θ_{MAX} on Pr have also not been predicted by the current models. Clearly more work is needed to elucidate the role of Pr in turbulent convection.

TABLE I. A comparison of the two experiments at $\mathrm{Ra} = 1 \times 10^9$.

	Pr=6.6	Pr=0.7
λ_{th}/L	0.010	0.007
λ_m/L	0.05	0.04
λ_{sk}/L	0.11	0.12
$\mathrm{Nu}_{\mathrm{pt}}$	48±6	76±11
$\theta_{\mathrm{max}}/\Delta$	0.060	0.058
Re_λ	50	600
Re_L	1100	15 400

APPENDIX C: ADVECTIVE HEAT TRANSPORT

In the regions of the cell away from the walls, advection is the most important means of heat transport. The total heat flux through the cell is related to how this transport is organized by the dynamics of the convective state. By making simultaneous measurements of temperature and velocity in water, as shown in Fig. 18, we study the advective transport. Because the heat flux through any horizontal plane in the cell is the same, local measurements made along the center axis pertain to the distribution of global transport. The vertical heat flux per unit time is written as $J(z) = \rho C_p \langle w \delta T \rangle - \chi \partial \langle T \rangle / \partial z$, where $w(z,t)$ is the vertical component of the fluctuating velocity, and $\delta T(z,t)$ is the variation of the temperature from the mean [37]. We neglect $\partial \langle T \rangle / \partial z$ in the bulk region, and measure the change in convective transport $\langle w \delta T \rangle$ with position.

Our measurements are made in water at $\mathrm{Ra} = 1.1 \times 10^9$, at heights ($z/L$): 0.016, 0.137, 0.383, and 0.492. The velocity is measured using the pH technique described in the text, and local temperature is measured as in the gas. The electrode for the velocity measurement and thermistor are 2 mm apart, so that the velocity is approximately the same at both detectors [12]. For $z/L \sim 1.6\%$, which is about $1.5\lambda_{\mathrm{th}}$, we find that the convective heat flux is approximately equal to the heat flux at the wall (the pointwise Nusselt number). From 14 to 49% of the cell height L, however, the convective heat flux is less than 5% of the heat flux at the wall. This means that most of the heat is being transported along the sides of the cell. Thus although the vertical heat flux at the center is still substantial at a few boundary layer thicknesses from the plate, it is negligible in the central region.

We can begin to study the dynamics of advective heat transport in the simultaneous traces of temperature and velocity. At $z/L \sim 1.6\%$, there is a correlation between peaks in the vertical velocity and temperature traces. At $z/L \sim 14\%$, strong temperature fluctuations correspond to velocity fluctuations, but there are also prominent peaks in the velocity trace with no accompanying occurrence in the temperature (Fig. 18). This is due to the fact that the velocity field is smoother than the tempera-

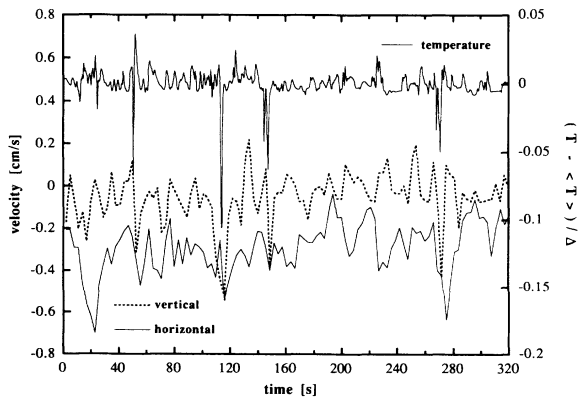

FIG. 18. Simultaneous traces of temperature and velocity (vertical and horizontal) at $z/L = 0.137$, for water at $\mathrm{Ra} = 1.1 \times 10^9$.

ture field [12]; there are eddies larger than the plumes. At both positions, the horizontal velocity is correlated with the temperature such that fluid warmer than average is moving faster than average. At $z/L \sim 38$ and 49%, peaks in one trace (temperature, vertical or horizontal velocity) almost always coincide with peaks in other traces. However, warm fluid does not necessarily rise nor does cold fluid always fall. In conclusion, the temperature fluctuations are driving the flow within 15% of the plate, but velocity fluctuations also occur in this region without a temperature signature. In the central region of the cell, the temperature behaves as a passive scalar.

APPENDIX D: HEAT TRANSPORT: LARGE SCALE FLOW OR THERMAL PLUMES?

Any attempt to understand the scaling $\mathrm{Nu} \sim \mathrm{Ra}^{2/7}$ must begin by addressing the question: how is heat transported out of the thermal layer? The model of Shraiman and Siggia [9] employs a local relationship between the heat flux and the advection of heat by the large scale circulation. Their assumption is that the heat flux into the thermal layer at each point along the plate is carried completely by the mean flow. In this appendix we will review their assumptions and results, and discuss relevant experiments. Using our measurements of the thermal boundary layer and the velocity profile at the center of the cell, we check their assumption, finding that the heat flux cannot be completely advected by the flow. Our measurements are made in water for $\mathrm{Ra} = 1 \times 10^9$, within the regime in which the 2/7 scaling is observed [4,31].

To begin with, the z axis is perpendicular to the plate, and the x axis is along it. The shear at the plate is defined as $\gamma \equiv (\partial U/\partial z)|_{z=0}$, where U is the mean velocity in the x direction. The assumptions made are that γ does not change along the plate (in x), that the velocity profile is linear close to the plate (leading to $U = \gamma z$), and that the thermal boundary layer occurs within this linear dependence. These assumptions imply that the heat which has come in through the plate must be carried horizontally by the mean flow. The result is a local relation between heat flux and shear at the plate:

$$\mathrm{Nu}_{\mathrm{pt}} = 0.27 \frac{L}{(\kappa x_0/\gamma)^{1/3}} \tag{D1}$$

where L is the height of the convection cell, κ is the thermal diffusivity, and x_0 is the distance along the plate from some effective starting point of the boundary layer, the downstream distance. Note that although γ is constant along the plate (in x), the thickness of the thermal boundary layer (and $\mathrm{Nu}_{\mathrm{pt}} = L/2\lambda_{\mathrm{th}}$) depends on x_0. The coefficient 0.27 comes from the requirement that $(T - T_{\mathrm{top}})/\Delta \to 0.5$ as $z \to \infty$.

In our experiment on water at $\mathrm{Ra} = 1 \times 10^9$, we measure both $\mathrm{Nu}_{\mathrm{pt}}$ and $U(z)$ at the center of the plate. To calculate γ from our measurements, we first recall that the large scale circulation in a cubic cell travels along the diagonal [12,26]. Our measurements of U, shown in Fig. 7, are made parallel to the side walls as described in Sec. III. Multiplying these measured velocities by $\sqrt{2}$, we find $\gamma = 1.88\ \mathrm{sec}^{-1}$. We also measure $\mathrm{Nu}_{\mathrm{pt}} \sim 50$ [12]. Putting these numbers into Eq. (D1), we calculate x_0 to be about 1–2 cm, a very small number considering that the flow sweeps across the whole plate. Although we do not measure x_0, we would expect $x_0 \sim L \times \sqrt{2}/2$ (about 13 cm) for measurements made at the center of the plate. Using $x_0 \sim 13$ cm in Eq. (D1) gives $\mathrm{Nu}_{\mathrm{pt}} \sim 23$, half of the measured flux. Thus the large scale circulation is too weak to balance the actual heat flux, contrary to the hypothesis used to derive the 2/7 scaling [9].

If the total heat is not carried by the shear, where does it go? It must then be carried normal to the plate, by thermal plumes and other active detachments. Transport normal to the plate can only be included if γ depends explicitly on x [38]. Local measurements of γ and λ_{th} at different positions along the plate is, to our knowledge, an untouched area in the study of thermal turbulence.

In a recent experimental paper, in which the local thickness of the thermal layer was measured with an optical technique, a different approach is taken to testing Eq. (D1) [31,32]. The constant coefficient in the equation is fit to the data as 0.66, instead of the value 0.27 used here. They confirm the dependence $\mathrm{Nu}_{\mathrm{pt}} \sim \gamma^{1/3}$, but have averaged out the x dependence of their local heat flux measurements. A more stringent check of the assumptions leading to Eq. (D1) would be to test the local prediction $\mathrm{Nu}_{\mathrm{pt}} \sim x_0^{-1/3}$.

Experimental evidence for the importance of plumes in the heat flux was seen in the enhanced shear experiments of Solomon and Gollub [4]. For $\mathrm{Ra} \sim 10^6$–10^8, they artificially impose a large scale flow in a water convection cell. They find that the imposed circulation balances the heat flux into the cell, but the imposed shear velocities are larger than the naturally occurring large scale circulation. More importantly, for cases in which this balance was realized, a *complete suppression of boundary layer detachments* was observed. The natural large scale circulations coexists with the emission of plumes, and the quantitative comparison presented above indicates that both advection (horizontal) and plumes (vertical) are important to the principle which determines the boundary layer thickness. In order to uncover this principle, we should begin by addressing the origin of the large scale circulation itself.

[1] W. V. R. Malkus, Proc. R. Soc. London Ser. A **225**, 185 (1954); G. E. Willis and J. W. Deardorff, Phys. Fluids **10**, 1861 (1967); T. Y. Chu and R. J. Goldstein, J. Fluid Mech. **60**, 141 (1973); D. C. Threlfall, *ibid.* **67**, 17 (1975); F. Heslot, B. Castaing, and A. Libchaber, Phys. Rev. A **36**, 5870 (1987).

[2] B. Castaing, G. Gunaratne, F. Heslot, L. Kadanoff, A. Libchaber, S. Thomae, X. Z. Wu, S. Zaleski, and G. Zanetti, J. Fluid Mech. **204**, 1 (1989).

[3] X. Z. Wu, Ph.D thesis, University of Chicago, 1991 (unpublished).

[4] T. H. Solomon and J. P. Gollub, Phys. Rev. A **43**, 6683

(1991).
[5] R. Krishnamurti and L. N. Howard, Proc. Natl. Acad. Sci. U.S.A. **78**, 1981 (1981).
[6] M. Sano, X. Z. Wu, and A. Libchaber, Phys. Rev. A **40**, 6421 (1989).
[7] D. B. Thomas and A. A. Townsend, J. Fluid Mech. **2**, 473 (1957); J. W. Deardorff and G. E. Willis, *ibid.* **28**, 675 (1967).
[8] W. V. R. Malkus, Proc. R. Soc. London Ser. A **225**, 196 (1954); L. N. Howard, in *Proceedings of the 11th International Congress of Applied Mechanics, Munich, Germany,* edited by H. Goertler (Springer, Berlin, 1966).
[9] B. I. Shraiman and E. D. Siggia, Phys. Rev. A **42**, 3650 (1990).
[10] T. H. Solomon and J. P. Gollub, Phys. Rev. Lett. **64**, 2382 (1990).
[11] A. Belmonte, A. Tilgner, and A. Libchaber, Phys. Rev. Lett. **70**, 4067 (1993).
[12] A. Tilgner, A. Belmonte, and A. Libchaber, Phys. Rev. E **47**, 2253 (1993).
[13] Designed by E. Moses at the University of Chicago.
[14] RTE-8DD refrigerated circulating bath, Neslab Instruments, Newington, NH.
[15] 70-Ω foil resistance heater, Minco Products, Minneapolis, MN.
[16] *Matheson Unabridged Gas Data Handbook* (Matheson Gas Products, East Rutherford, NJ, 1974).
[17] L. Adler and C. Yaws, Solid State Technol. **18**, 35 (1975); J. Hoogland, H. Van Den Berg, and N. Trappeniers, Physica **134A**, 169 (1985); J. Kestin and N. Imaishi, Int. J. Thermophys. **6**, 107 (1985); SF_6 Thermodynamic Tables, Allied-Signal Inc., Morristown, NJ (1991).
[18] D. J. Tritton, *Physical Fluid Dynamics,* 2nd ed. (Clarendon, Oxford, 1988).
[19] Type BB05, Thermometrics Inc., Edison, NJ.
[20] Model 16828 Motorized Translator, with model 18008 controller, Oriel Corporation, Stratford, CT.
[21] Model 124A or model 5207 Lock-In Amplifier, Princeton Applied Research, Princeton, NJ.
[22] HP 3562A Dynamic Signal Analyzer, Hewlett-Packard Co., Everett, WA.
[23] D. J. Baker, J. Fluid Mech. **26**, 573 (1966); W. Merzkirch, *Flow Visualization* (Academic, New York, 1987).
[24] X. Z. Wu, L. Kadanoff, A. Libchaber, and M. Sano, Phys. Rev. Lett. **64**, 2140 (1990).
[25] The profile for f_c for gas is more precise than for water (Fig. 9), due to the fact that the power spectrum extends to higher frequencies for gas (the flow is faster). Thus the statistics are better for data taken over the same length of time.
[26] G. Zocchi, E. Moses, and A. Libchaber, Physica A **166**, 387 (1990).
[27] From this argument, it is unusual that f_{cMAX} scales for $Ra < 2\times 10^7$, where the Ra dependence of λ_{th} has changed. However, from previous observation we know that the Ra dependence of the large-scale circulation speed has also changed (see Ref. [6]), in a direction that would compensate for the change in λ_{th}.
[28] Based on conversations with B. Shraiman and E. Siggia (private communication).
[29] E. Siggia (private communication).
[30] R. Kraichnan, Phys. Fluids **5**, 1374 (1962).
[31] F. Chillà, S. Ciliberto, and C. Innocenti, Europhys. Lett. **22**, 681 (1993).
[32] F. Chillà, S. Ciliberto, C. Innocenti, and E. Pampaloni, Nuovo Cimento **15**, 1229 (1993).
[33] C. H. B. Priestley, Aust. J. Phys. **7**, 176 (1954).
[34] S. Globe and D. Dropkin, J. Heat Transfer **81**, 24 (1959).
[35] B. J. Gluckman, H. Willaime, and J. P. Gollub, Phys. Fluids **5**, 647 (1993).
[36] E. D. Siggia, Ann. Rev. Fluid Mech. **26**, 137 (1994).
[37] H. Tennekes and J. L. Lumley, *A First Course in Turbulence* (MIT Press, Cambridge, 1972).
[38] Because of the incompressibility condition $(\partial u/\partial x)+(\partial w/\partial z)=0$ and the condition $w=0$ at the plate, one can only have $w\neq 0$ everywhere if $u=u(x,z)$, and not just $u=u(z)$ as in Ref. [9].

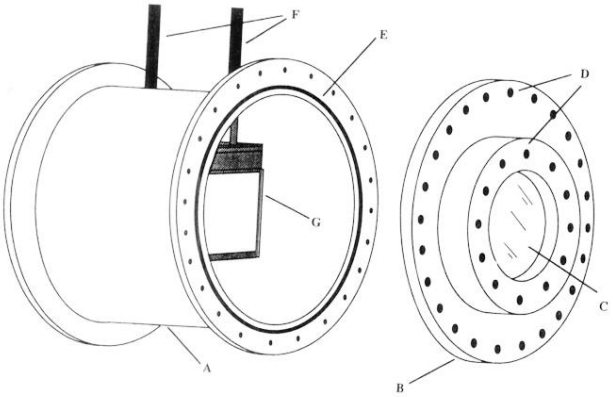

FIG. 1. A diagram of the experimental apparatus for compressed gas: *A*, steel pressure vessel; *B*, endcap; *C*, plexiglass window; *D*, bolts; *E*, *o* ring; *F*, water supply pipes; and *G*, convection cell.

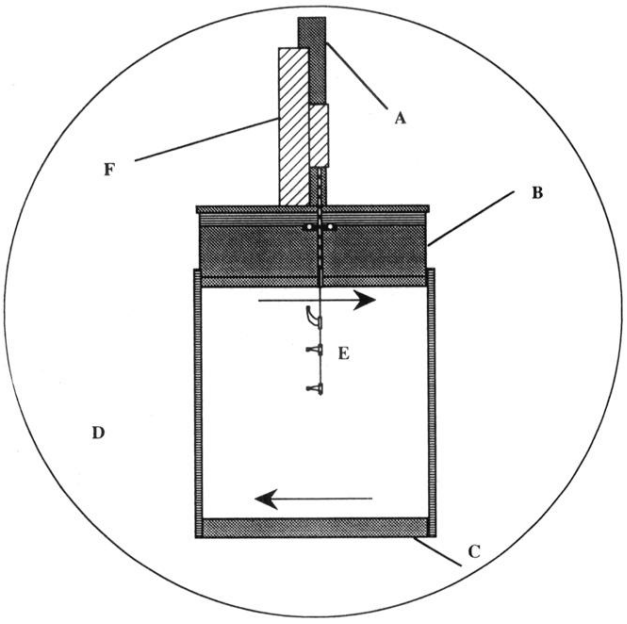

FIG. 2. A diagram of the gas convection cell: *A*, water supply pipes; *B*, top plate; *C*, bottom plate; *D*, exterior filled with cotton; *E*, thermistors on tube (not to scale); and *F*, translation stage. The arrows are drawn to indicate the direction of the large scale circulation near the plates.